Epitaxial growth and magnetic characterization of EuSe thin films with various crystalline orientations Ⓕ

Ying Wang, Ⓘ**D Xinyu Liu,** Ⓘ**D Seul-Ki Bac, et al.**

COLLECTIONS

Ⓕ   This paper was selected as Featured

View Online   Export Citation   CrossMark

ARTICLES YOU MAY BE INTERESTED IN

Strength softening mitigation in bimodal structured metals
Journal of Applied Physics **131**, 045102 (2022); https://doi.org/10.1063/5.0075475

Quantum delegated computing ciphertext retrieval scheme
Journal of Applied Physics **131**, 044401 (2022); https://doi.org/10.1063/5.0080097

Applicability of coherent x-ray diffractive imaging to ferroelectric, ferromagnetic, and phase change materials
Journal of Applied Physics **131**, 040901 (2022); https://doi.org/10.1063/5.0072399

Epitaxial growth and magnetic characterization of EuSe thin films with various crystalline orientations

Ying Wang,[1] Xinyu Liu,[2] Seul-Ki Bac,[2] Jiashu Wang,[2] Jacek K. Furdyna,[2] Badih A. Assaf,[2]
Maksym Zhukovskyi,[3] Tatyana Orlova,[3] Valeria Lauter,[4] Neil R. Dilley,[5] and Leonid P. Rokhinson[1,5,6,a]

AFFILIATIONS

[1] Department of Physics and Astronomy, Purdue University, West Lafayette, Indiana 47907, USA
[2] Department of Physics, University of Notre Dame, Notre Dame, Indiana 46556, USA
[3] Notre Dame Integrated Imaging Facility, University of Notre Dame, Notre Dame, Indiana 46556, USA
[4] Neutron Scattering Division, Neutron Sciences Directorate, Oak Ridge National Laboratory, Oak Ridge, Tennessee 37831, USA
[5] Birck Nanotechnology Center, Purdue University, West Lafayette, Indiana 47907, USA
[6] Department of Electrical and Computer Engineering, Purdue University, West Lafayette, Indiana 47907, USA

[a] Author to whom correspondence should be addressed: leonid@purdue.edu

ABSTRACT

We report different growth modes and corresponding magnetic properties of thin EuSe films grown by molecular beam epitaxy on BaF_2, $Pb_{1-x}Eu_xSe$, GaAs, and Bi_2Se_3 substrates. We show that EuSe grows predominantly in the (001) orientation on GaAs(111) and Bi_2Se_3, but along the (111) crystallographic direction on BaF_2 (111) and $Pb_{1-x}Eu_xSe$ (111). High resolution transmission electron microscopy measurements reveal a sharp and highly crystalline interface for both (001) and (111) EuSe films. In agreement with previous studies, ordered magnetic phases include antiferromagnetic, ferrimagnetic, and ferromagnetic phases. In contrast to previous studies, we found a strong hysteresis of the antiferromagnetic–ferrimagnetic transition. The ability to grow epitaxial films of EuSe on Bi_2Se_3 and of Bi_2Se_3 on EuSe enables further investigation of interfacial exchange interactions between various phases of an insulating metamagnetic material and a topological insulator.

Published under an exclusive license by AIP Publishing. https://doi.org/10.1063/5.0075827

INTRODUCTION

A renewed interest in magnetic insulators (MIs), such as europium chalcogenides, is motivated by a possibility to induce strong spin splitting in heterostructured materials via proximity exchange interactions.[1] One of the most interesting applications of strong interfacial Zeeman fields is a possibility to locally control topological surface states (TSS) in topological insulators (TIs).[2,3] For example, selective gapping of top and bottom TSS is needed to realize the quantum anomalous Hall effect[4,5] and gapping of side TSS, and, thus, electrically disconnecting top and bottom TSS will benefit future spintronic devices,[6] while local gapping of TSS is required to localize non-Abelian excitations in TI-based topological superconductors.[7] Strong interfacial exchange requires the formation of clean epitaxial interfaces with controllable crystallographic

orientation and atomic arrangement, which motivates growth and characterization of MI/TI heterostructures reported in this paper.

Opening of the exchange gap in the Dirac spectrum of TSS has been reported in Bi_2Se_3/EuS heterostructures.[8] Polarized neutron reflectometry detected interfacial magnetization in these heterostructures up to room temperature, 20 times higher than the Curie temperature $T_c = 17$ K of the bulk EuS.[9] In Cr_2Te_3/Bi_2Te_3/Cr_2Te_3 ferromagnet–TI heterostructures, one of the interfaces demonstrated magnetic textures and non-uniform gapping of TSS.[10] Gapping of TSS by exchange-coupling to an antiferromagnetic insulator has an advantage of reducing stray magnetic fields from the bulk of the magnetic material and has been demonstrated in magnetically doped TI interfacing Cr_2O_3[11] and CrSb.[12,13] At present, there are no reports of both top and bottom TSS modulations in non-magnetic TIs.

EuSe is an insulating metamagnetic material that exhibits a variety of magnetic phases in a narrow range of magnetic fields.[14] Almost perfect cancellation of the nearest and next-nearest neighbor interactions between localized magnetic moments on the half-filled 4f levels of Eu2+ ions leads to a phase diagram that includes several antiferromagnetic (AF-I ↑↓↑↓, AF-II ↑↑↓↓), ferrimagnetic (FIM ↑↑↓), and ferromagnetic (FM) phases in the bulk, where magnetization vectors are confined to {111} planes of the NaCl-type crystal structure (as shown in Fig. 1). The magnetic moments of Eu atoms are ferromagnetically aligned within the {111} planes. AF sheets are stacked in a collinear AF order.[15] There are two types of AF domain walls: T (twin)-domain and S (spin)-domain. Each of the four possible [111] stacking directions determines the T-domain. A single T-domain crystal has a triclinic symmetry with an easy axis along one of three [211] derived directions, $[\bar{2}11]$, $[1\bar{2}1]$, and $[11\bar{2}]$ with spins laying within a {111} plane.[16–18] Each of the three $[11\bar{2}]$ spin directions per T-domain defines an S-domain.[19] It has been shown that T-domains can be eliminated by applying momentary pressure along the (111) direction or a large (>0.2 T) external magnetic field.[20] Thus, it is of great interest to control the orientation of EuSe during molecular beam epitaxy (MBE) growth to enable proximity to FM (111) and FM or AF (100) surfaces. The relative strength of the magnetic phases and the positions of the phase boundaries are also highly sensitive to strain and can be tuned during epitaxial growth.[21,22] The magnetic properties of bulk EuSe[23,24] and thin (111) layers[21] have been studied in the past, and exchange-enhancement of the Zeeman splitting in Al has been reported in Al/EuSe/Ag tunnel junctions.[25] EuSe itself has optical absorption properties that are very sensitive to magnetic fields.[14,26]

In this work, we report the growth and characterization of thin EuSe with various crystalline orientations obtained on a variety of substrates including Bi$_2$Se$_3$. Using the adapted growth conditions, we

achieve the growth of a (001)-oriented EuSe layer on GaAs(111)B and Bi$_2$Se$_3$. We also synthesized (111) oriented EuSe films on lattice-matched BaF$_2$ (111) and a (Pb,Eu)Se pseudosubstrate for comparison. We performed superconducting quantum interference device (SQUID) magnetometry and constructed magnetic phase diagrams for the (001) and (111) EuSe films. The (111)-oriented layers yield a phase diagram similar to previous studies, albeit we observe large hysteresis for the FIM–AF transition. Magnetization in the (001) layers shows a strong contribution from the hard axis since both in-plane and out-of-plane directions do not coincide with the easy axes oriented in the (111) plane (Fig. 1). Knowledge of this phase diagram is important for interpreting proximity effect experiments with compensated (001) EuSe surfaces.

MATERIAL GROWTH

The EuSe films are grown by MBE on three types of substrates and buffer layers: (SA) lattice-mismatched GaAs, (SB) nearly lattice-matched BaF$_2$ (111), (SC) Pb$_{1−x}$Eu$_x$Se/BaF$_2$ (111) pseudo-substrates, and (SD1) van der Waals TI Bi$_2$Se$_3$ grown on sapphire. Table I summarizes parameters of the samples. High-purity PbSe compound flux and Eu, Bi, and Se elemental fluxes are obtained from standard effusion cells. The growth is monitored by *in situ* reflection high energy electron diffraction (RHEED). The growth is carried out under Se-rich conditions. The Se flux is kept constant at the beam equivalent pressure (BEP) ratio of Se:Eu of 4−20. Under these conditions, the growth rate of EuSe (1–2 nm/min) is controlled by the Eu flux. During the growth process, the substrate temperature is maintained close to 300 °C. Note that the actual surface temperature can depend on the thermal conductivity of each specific substrate. However, in past studies, growth temperatures between 260 °C (Ref. 27) and 420 °C (Ref. 28) have successfully been used. Various substrate treatments are carried out prior to the deposition of EuSe.

For GaAs (111)B substrates, a specific treatment with Se is carried out prior to the growth. First, a GaAs (111)B substrate is heated to ~570 °C for removing native oxide. Next, the substrate is annealed under Se flux (~2 × 10$^{−6}$ Torr) at 600 °C for 20 min to obtain streaky (1 × 1) RHEED pattern. Se passivation smoothens the surface and terminates it with Se bonds. EuSe grown on the GaAs (111)B substrate has two initiation processes. Growth on GaAs without a buffer layer often yields a three-dimensional growth mode with a rough surface, as seen in Fig. 2(a). Alternatively, a specific atomic-layer-epitaxy (ALE) growth process is performed to initiate epitaxial layer-by-layer growth mode: the growth is initiated by deposition of six periods of Se monolayers followed by a monolayer of Eu at lower temperature (200 °C). Then, the substrate is gradually heated to 300 °C, and a nice streaky RHEED pattern [not shown, similar to Fig. 2(b)] appears prior to the MBE growth of the EuSe film. A latter process with a higher Se:Eu flux ratio yields uniform EuSe in the (001) growth direction with a 12-fold symmetry RHEED pattern, which suggests that the four EuSe {100} planes are parallel (aligned) to the three {110} GaAs (111) planes, similar to what was recently reported for the growth of PbSe on GaAs[29] [see also Fig. S2(b) in the supplementary material].

We also performed EuSe growth on Bi$_2$Se$_3$ grown on sapphire c-plane (sample SD1) or GaAs (111)B (SD2) substrates. 15–20 nm
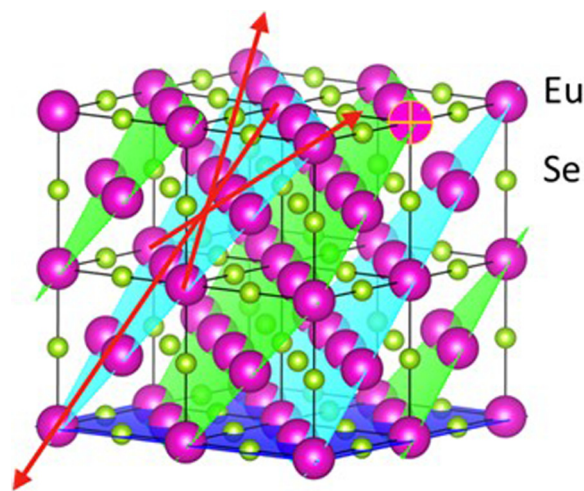

FIG. 1. Crystal structure of EuSe. The magnetization vector lies in one of four {111} planes (T-domains), which are marked by green and cyan planes; red arrows indicate three possible magnetization easy axes in the {111} planes for each T-domain (S-domains).

TABLE I. Properties of EuSe films studied in this work. Film thickness is determined from MBE growth calibration and confirmed for several films using TEM imaging. The root mean square (RMS) surface roughness R_a is extracted from atomic force microscopy (AFM) images. The dominant crystal orientation is determined by XRD. Rare (111) inclusions are detected by TEM but not by XRD. The Néel temperature is extracted from the temperature dependence of magnetic susceptibility. Out-of-plane strain is calculated by comparing the out-of-plane lattice constant measured by XRD to the bulk lattice constant. AFM images used to extract R_a are shown in the supplementary material.

Growth direction	Growth sequence (sample ID)	Thickness (nm)	R_a(nm)	T_N (K)	Strain	Note on growth
(001)	GaAs(111)B/EuSe (SA1)	120	2.96	5.1	0%	Se:Eu = 10, pseudo 2D
Mixed	GaAs(111)B/EuSe (SA2)	120		5.4	+0.09%	Se:Eu = 4
(001)	Sapphire/Bi$_2$Se$_3$/EuSe (SD1)	16.6/20	0.90	4.4	−0.08%	
(001)	GaAs(111)B/Bi$_2$Se$_3$/EuSe (SD2)	18/16	1.74	4.4	+0.1	
(111)	BaF$_2$(111)/EuSe (SB)	90	2.58	4.9	−0.09%	Rough surface initially
(111)	BaF$_2$(111)/pseudo-substrate^a/EuSe/Bi$_2$Se$_3$ (SC)	164/20/28	0.98	5.5	+0.65%	pseudosubstrate reestablishes 2D growth
Trilayer	EuSe/Bi$_2$Se$_3$/EuSe (SF)					See the supplementary material

^{a}Pseudosubstrate: PbSe (64 nm)/Pb$_{0.8}$Eu$_{0.2}$Se(57 nm)/Pb$_{0.58}$Eu$_{0.42}$Se(43 nm).

thick Bi$_2$Se$_3$ were grown at 300 °C under an Se-rich condition as in Refs. 30–32, followed by the EuSe growth. Under the Se-rich condition (Se:Eu > 10), the RHEED pattern is blurry but streaky, indicating a layer-by-layer growth mode [see Fig. 2(b)].

The BaF$_2$ and sapphire substrates are annealed *in situ* at 650–700 °C for at least 1 h for thermal cleaning. We find that EuSe on BaF$_2$ without a buffer layer is quasi-two-dimensional and yields a blurred and spotty RHEED pattern, as seen in Fig. 2(c), and a rough surface. An introduction of a graded Pb$_{1-x}$Eu$_x$Se buffer layer

FIG. 2. RHEED patterns of EuSe films grown on different substrates: (a) GaAs (111)B, (b)Bi$_2$Se$_3$, (c) BaF$_2$ (111), and (d) Pb$_{1-x}$Eu$_x$Se pseudosubstrate. The [110] plane spacing on the RHEED patterns is indicated by a white arrow. The direction of the beam is always perpendicular to the [110] direction of EuSe.

(from bottom to top $x = 0$, $x = 0.2$, and $x = 0.425$) restores 2D epitaxial growth, as indicated by the streaky RHEED pattern in Fig. 2(d). The growth of this buffer layer provides a surface that is isostructural with EuSe and is found to be ideal to initiate the growth of a thin layer of this material. An EuSe film grown on a gradient buffer is compressively strained, whereas all other growths yield relaxed layers.

STRUCTURAL CHARACTERIZATION

Structurally, the films are characterized by high resolution x-ray diffraction (HRXRD) on a six-angle diffractometer equipped with a 1.5406 Å $Cu\_K_{\alpha1}$ source. Transmission electron microscopy (TEM) measurements are also carried out and shown in the supplementary material. Figures 3 and 4 show the x-ray diffraction (XRD) characterizations revealing the growth direction and strain of EuSe thin films grown on various substrates. The growth of EuSe on GaAs (111)B yields two different types of samples: samples with a mixed phase with both EuSe (111) and EuSe (001), and a single phase with EuSe (001) shown in Figs. 3(a) and 3(b) for two different samples. The growth direction depends on the Se:Eu ratio: for Se:Eu > 10, a (001) growth is preferred (SA1), while for Se:Eu ∼ 4, a (001) growth with (111) inclusions is observed (SA2), as can be seen from both XRD spectrum and TEM images. The structural properties of EuSe grown on GaAs (111)B and the corresponding interface alignments are discussed in the supplementary material (Figs. S2 and S3).

Figure 3(b) shows the XRD patterns of EuSe grown on Bi$_2$Se$_3$. A strong (002) EuSe peak is observed, indicating that EuSe is predominantly (001) oriented. A wide-angle scan is included in the supplementary material, ruling out the formation of any phases in this layer other than EuSe. The lattice constant extracted from the (002) peak (6.186 Å) suggests that EuSe grows along the (001) direction and is fully relaxed in the c-plane of Bi$_2$Se$_3$ (001). The Bi$_2$Se$_3$ (006) peak also appears in the data and yields a lattice constant (28.511 Å) close to the lattice constant of bulk Bi$_2$Se$_3$.

The XRD pattern of EuSe grown on BaF$_2$ (111) is shown in Fig. 3(c). In this case, an EuSe layer with the (111) orientation is obtained, which is negligibly strained (<0.09%). The XRD pattern
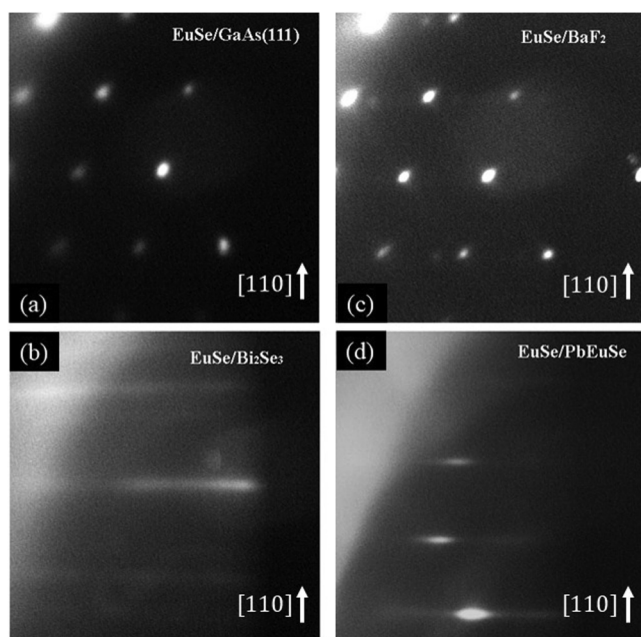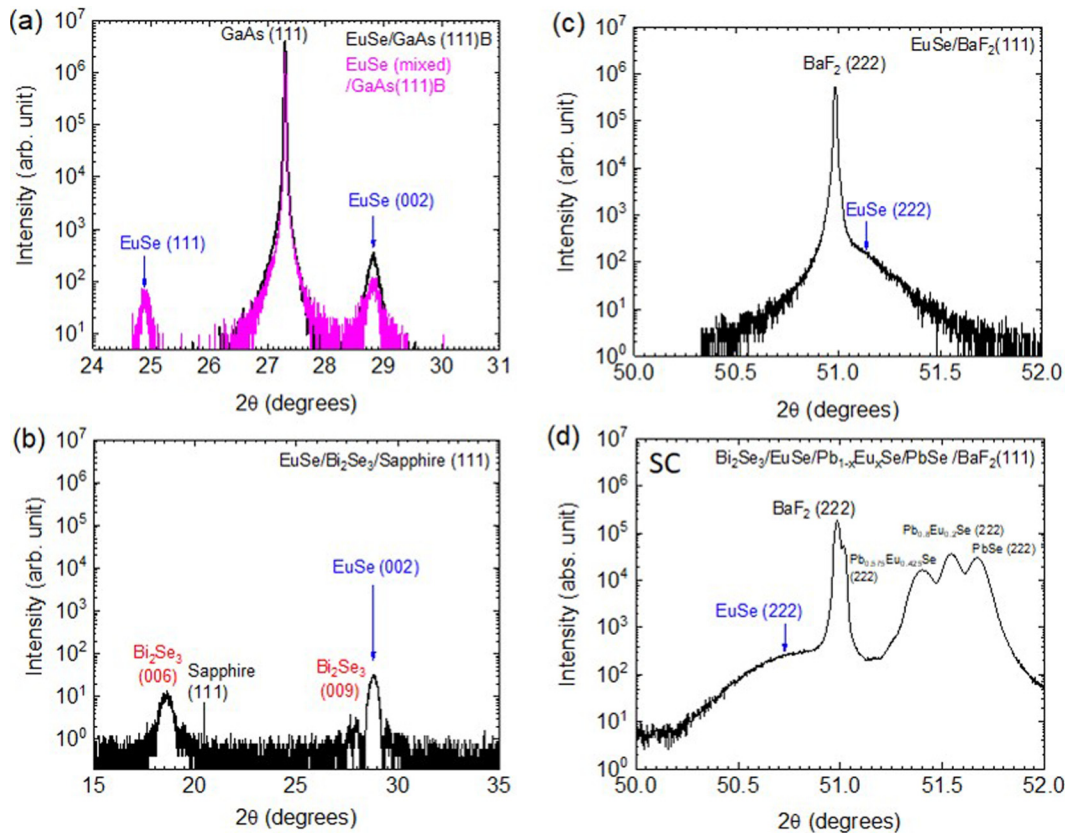
FIG. 3. Structural characterization of EuSe growth on various substrates. HRXRD of EuSe films grown on (a) GaAs (111)B, (b) Bi_2Se_3, (c) BaF_2 (111), and (d) $Pb_{1-x}Eu_xSe/BaF_2$ (111) substrates.

from EuSe grown on the $Pb_{1-x}Eu_xSe$ buffer layer is shown in Fig. 3(d). This layer is also (111) oriented but slightly compressively strained in-plane and tensile strained in the (111) direction (~0.6%).

To further understand the planar arrangement of the (001) EuSe with the C_4 symmetry of the surface on a Bi_2Se_3 surface with the C_3 symmetry, we carried out a φ-scan of {224} planes of the (001) EuSe. It exhibits a 24-fold periodic structure shown in Fig. 4(a). The origin of this structure can be understood as follows. The four EuSe {100} planes align with the three {110} planes of the Bi_2Se_3 (001) surface, forming a 12-fold periodic structure [Fig. 4(b)]. The four EuSe {110} planes can also align with the three {110} planes of the Bi_2Se_3 (001) surface, yielding an additional 12-fold periodic structure shifted by 15° [Fig. 4(c)]. This 24-periodic structure is contrasted with the threefold periodic pattern obtained from Bi_2Se_3. The type of alignment observed here is similar to the alignment found for the rock salt PbSe on zinc blende GaAs(111)B.[29] Thus, while the out-of-plane orientation of EuSe occurs predominantly along the (001) direction, two types of in-plane alignments are recovered. Rotated domains can also be resolved in the TEM image of EuSe(001) grown on Bi_2Se_3, shown in Fig. 4(d) confirming this conclusion.

Overall, XRD measurements clearly demonstrate growth in the (111) orientation on BaF_2 (111) and $Pb_{1-x}Eu_xSe$ (111) with a nearly matched lattice, as well as a mixed phase or a pure (001)-oriented growth on GaAs(111)B and the Bi_2Se_3 surfaces with a large lattice mismatch. This flexibility of crystallographic orientation can provide additional control of the magnetic exchange-coupling at the EuSe/Bi_2Se_3 interface and an additional knob to alter the properties of the TSS.

MAGNETIC PROPERTIES

The magnetic characterization of EuSe films is performed with a Quantum Design MPMS-3 SQUID magnetometer. More information on sample preparation and data analysis can be found in the supplementary material. This section is focused on the comparison of samples grown on BaF_2 and Bi_2Se_3. The temperature dependence of the magnetic susceptibility χ for BaF_2/EuSe and Bi_2Se_3/EuSe is plotted in Figs. 5(a) and 5(b), respectively. The Néel temperature $T_N = 4.4-4.9$ K for strain-free EuSe thin films SB and SD1 is found to be close to T_N in bulk crystals (4.6 K) and in thick epitaxial films (4.75 ± 0.25 K).[21] For EuSe (111), we also find that the in-plane $\chi_\parallel \to 0$ for $T \to 0$, while the out-of-plane $\chi_\perp$ remains

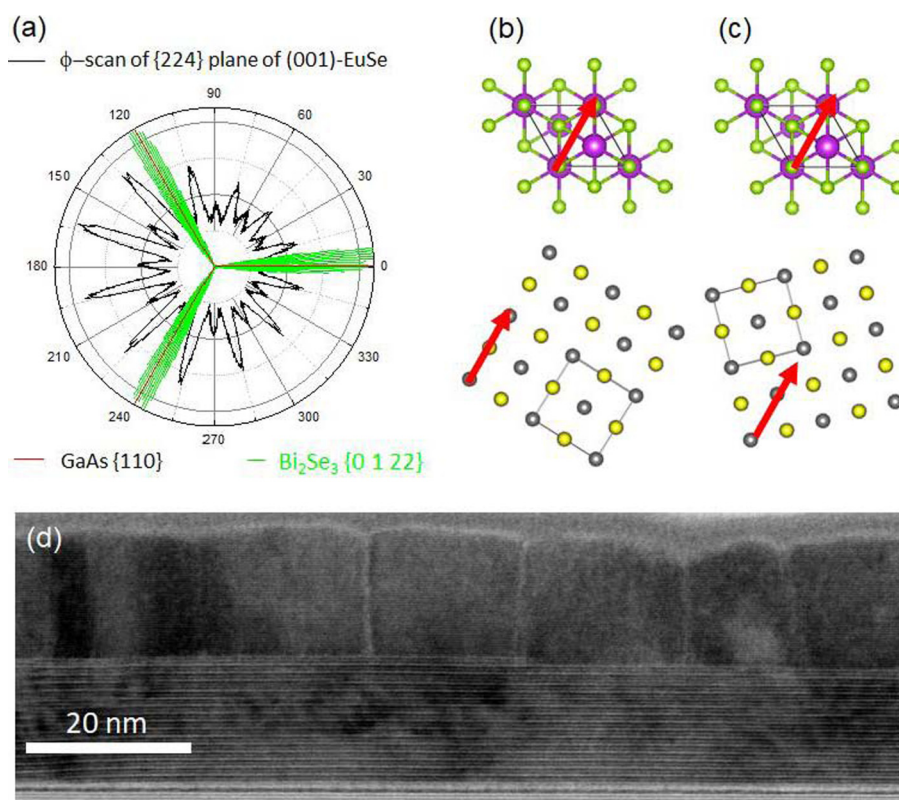**FIG. 4.** (a) Polar plot of a φ-scan of the (224) EuSe Bragg peak with (001) growth direction on Bi_2Se_3, and ϕ-scan of the {0 1 22} Bi_2Se_3 Bragg peak for sample SD1. (b) Alignment of the [100] direction of EuSe with a {110} direction of Bi_2Se_3. (c) Alignment of the [110] direction of EuSe with a {110} direction of Bi_2Se_3. (d) TEM of EuSe on Bi_2Se_3 showing grains with various in-plane orientations, consistent with the ϕ-scan.

finite [Fig. 5(a)]. This confirms that the magnetization at low fields lays in the (111) plane perpendicular to the growth axis. For (001) EuSe growth, both $\chi_\parallel$ and $\chi_\perp$ are finite in weak magnetic fields when $T \to 0$, as shown by dashed lines [Fig. 5(b)]. This is consistent with magnetic field pointing at an angle to the magnetization axis

for both directions of the field and indicates that the magnetization does not lie along the growth axis but remains in the (111) plane.

In Figure 6, we plot the magnetization loops M(H) normalized to fully magnetized Eu^{2+} (6.94 μ_B) for sample SD1. Magnetization loops are shown for different temperatures and for a field applied
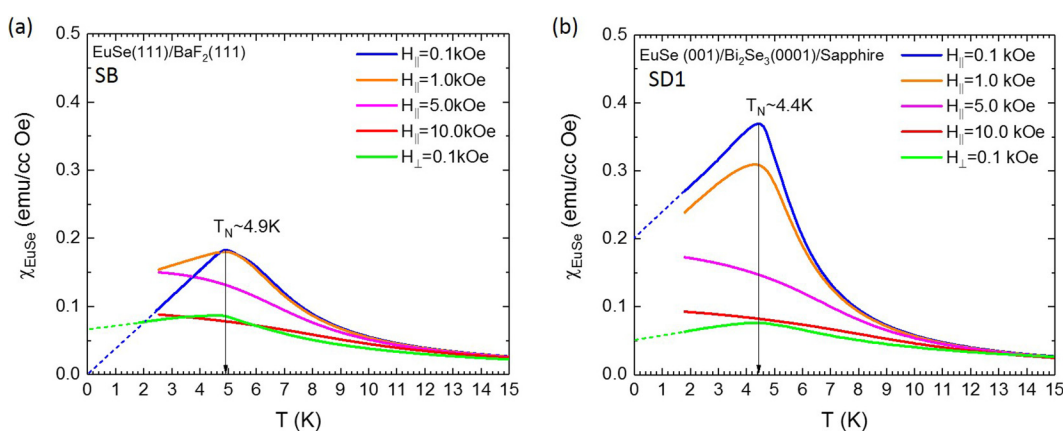

FIG. 5. Temperature dependence of magnetic susceptibilities of EuSe with in-plane $H_\parallel$ and out-of-plane $H_\perp$ magnetic fields for (a) EuSe (111) and (b) EuSe (001): Both samples show the evolution of magnetic properties from AF to FM when increasing the applied magnetic field. The dashed lines indicate a comparison of zero temperature susceptibilities at small $H_\parallel$ and $H_\perp$ for both samples.
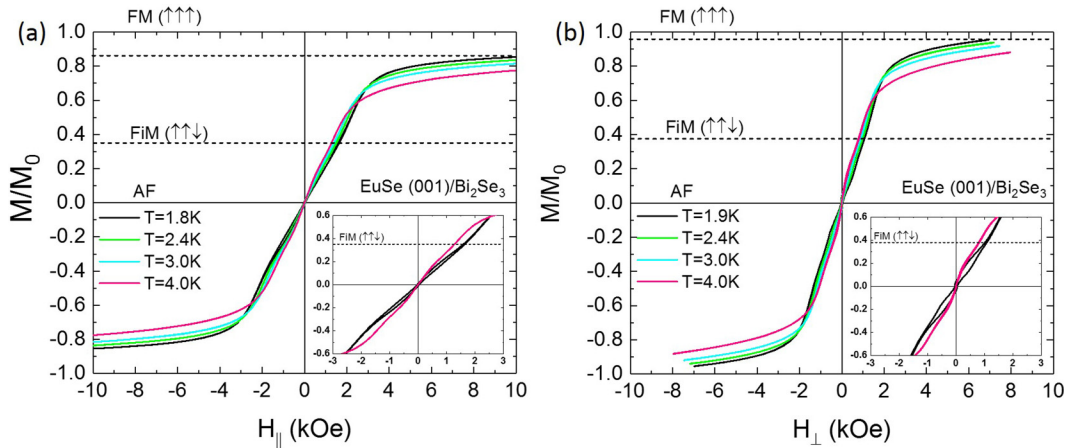
FIG. 6. Normalized magnetic moment per Eu^{2+} ion as a function of magnetic field at different temperatures for (a) $H_\parallel$ and (b) $H_\perp$ for EuSe (001) on van der Waals TI Bi_2Se_3 grown on sapphire. The saturation values of FM and FIM are indicated by dashed lines. Inset: hysteresis shown on an enlarged scale.

parallel ($H_\parallel$) and perpendicular ($H_\perp$) to the {001} planes. Magnetic transitions are more pronounced in the derivative plot (dM/dH), as shown in Fig. 7. The four peaks correspond to the expected phase transitions FM–FIM (A) and FIM–AF (B). In agreement

with previous reports, the FM–FIM transition is observed at $H(A) = 1.5–2.5$ kOe and is not hysteretic. The sharpness of this transition does not depend on the temperature, as can be seen from the almost T-independent height of the A peaks. It was
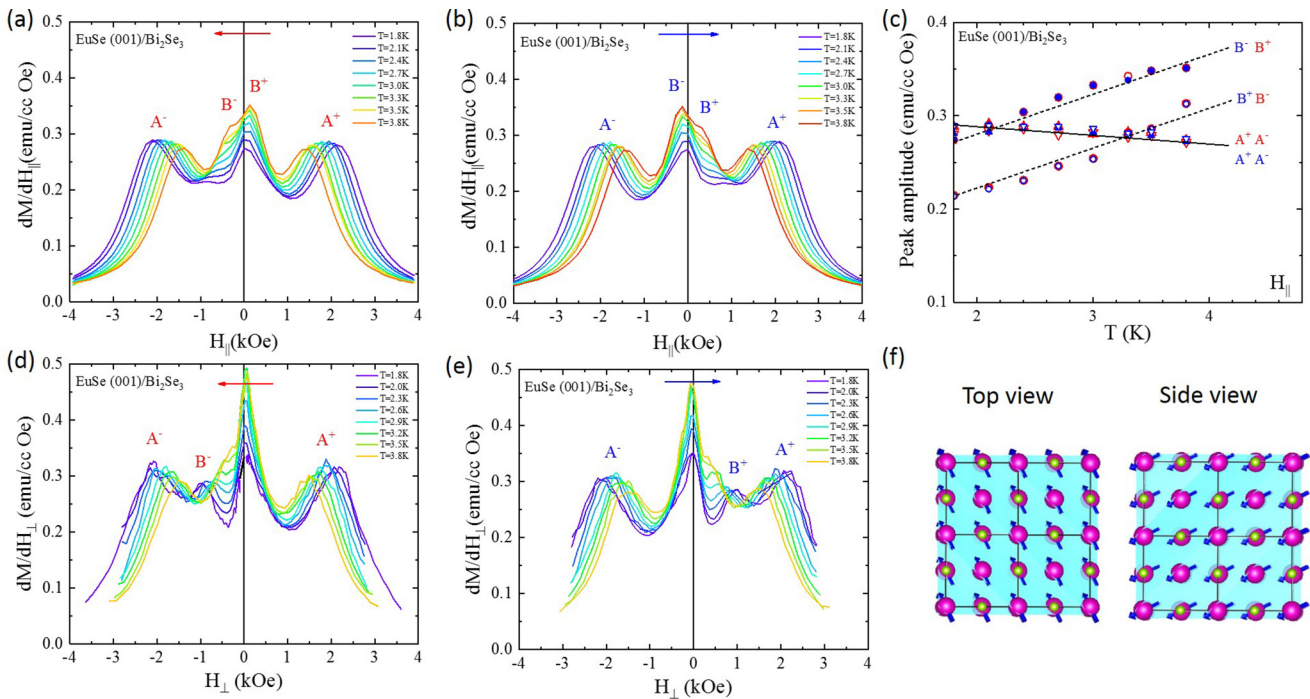

FIG. 7. Magnetic properties of EuSe (001) on Bi_2Se_3: Differential magnetic susceptibility (dM/dH) as a function of magnetic field with two opposite field sweep directions at different temperatures for in-plane $H_\parallel$ [(a) and (b)] and out-of-plane $H_\perp$ [(d) and (e)]: FM–FIM transitions are labeled by A^+ and A^- and guided by solid lines, AF–FIM transitions are labeled by B^+ and B^- and guided by dotted lines, and arrows indicate the field sweep direction corresponding to the dM/dH curves; (c) An amplitude of peaks A and B is plotted as a function of temperature; (f) EuSe (001) crystal structure with a magnetization plane (cyan color) and spin rotation (blue arrows).

unexpectedly found that the AF–FIM transition (peaks B) is strongly hysteretic; the hysteresis is emphasized in Fig. 7(a), where the upward sweep (dashed line) is overlapped with the downward sweep curves. The temperature dependence of peak B indicates that the AF–FIM transition broadens with the temperature decrease. The presence of a peak around $H = 0$ confirms that in thin (001) EuSe films, magnetization is retained within the {111} planes. For $H_\perp$, the differential magnetic susceptibility shows a larger peak centered at $H_\perp = 0$, which indicates a stronger out-of-plane canting of the spins. The magnetic susceptibility of EuSe (001) films is a combination of the in-plane and out-of-plane responses of the EuSe (111) film (see the supplementary material). Therefore, the observation of peak A (and peak B), which corresponds to the FM–FIM (and AF–FIM) transitions, is almost identical for both $H_\parallel$ and $H_\perp$.

Using the field dependence of peaks A and B, we construct and compare the magnetic phase diagrams of EuSe (001) and EuSe (111) thin films in Fig. 8. Both thin films show similar phase diagrams. For EuSe (111) [see Figs. 8(c) and 8(d)], we observe an

increase in the field values by ≈20% for FM–FIM compared to the purple lines, which show the phase boundaries in bulk EuSe (111), extracted from Ref. 21. In bulk samples, two distinct AF regions with different magnetic periodicities are observed above 3.6 and below 2.8 K, and the AF phase is not formed in the temperature range of 2.8–3.6 K. In thin films, we found that the AF–FIM transition is present for all $T < T_N$, and the transition field $H_\parallel(B^-)$ for field sweeping down *increases* uniformly with decreasing T. The value $H_\parallel(B^-) \approx 0.4 H_\parallel(A)$ of the FM–FIM transition and has a similar dependence on T. On the contrary, $H_\parallel(B^+)$ for the FIM–AF transition *decreases* with decreasing T; $H_\parallel(B^+) \approx 0$ for $T < 3.2$ K. A small hysteresis in the bandgap energy as a function of magnetic field has been reported in μm-thick films;[33] the large hysteresis in the current work (≈1 kOe) can be attributed to the strongly reduced film thickness compared to the previous work. The strong dependence of the dynamics of the phase transition on the film thickness and the presence of surfaces has been extensively studied for the AF–FM transition, which occurs near room temperature in FeRh alloys.[34–36] Such a strong modification of the AF–FIM
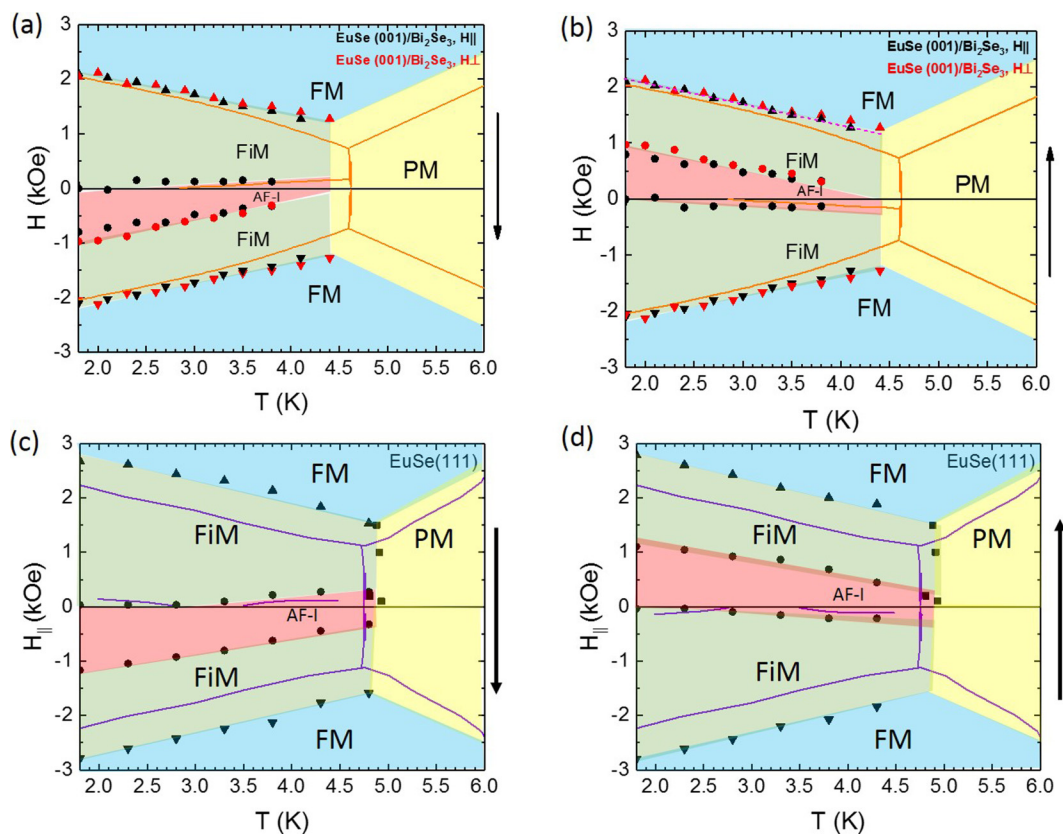

FIG. 8. Phase diagram of EuSe (001) on Bi$_2$Se$_3$ for (a) field sweeping down and (b) field sweeping up. In-plane phase diagram of EuSe (111) on nearly lattice-matched BaF$_2$ (111) for (c) field sweeping down and (d) field sweeping up. Dots and triangles are the positions of peaks A and B in Fig. 7. Black and red symbols indicate $H_\parallel$ and $H_\perp$, respectively. The red, green, blue, and yellow areas represent the AF, FIM, FM, and paramagnetic (PM) regions, respectively. The arrows indicate the directions of the field sweep. For a comparison, the purple lines are phase boundaries for a bulk μm-thick EuSe (111) (data from Ref. 21) and orange lines are phase boundaries for a single crystal EuSe (001) (data from Ref. 23).

transition in thin EuSe films can also affect the strength of the EuSe/TI magnetic exchange.

CONCLUSIONS

In summary, we have studied the structural and magnetic properties of thin EuSe epilayers grown on various substrates and buffer layers. EuSe grows in the (001) direction on both GaAs(111) B and Bi_2Se_3 substrates with good morphology. On BaF_2 (111), EuSe grows in the (111) direction in the quasi-2D growth mode, which leads to the formation of a rough surface. The introduction of $Pb_{1-x}Eu_xSe$ buffer layers improves the surface morphology. The magnetic phase diagram for thin films has AF, FIM, and FM phases similar to bulk crystals. The field value for the FIM–FM transitions is slightly enhanced compared to the bulk one, while the AF–FIM transition is highly hysteretic and has a T-dependence that is different from bulk crystals. Controlling the dynamics of the phase transition is the key for the successful realization of selective gaping of TSS in magnetic material/TI heterostructures. The observed enhancement of the AF–FIM transition and strong hysteresis may provide a useful means to control magnetic order and phase transition by tuning the film thickness. The growth of (001) EuSe on Bi_2Se_3 and GaAs (111)B makes it possible to realize an AF interface with a TSS.

SUPPLEMENTARY MATERIAL

The supplementary material includes atomic microscopy images of devices listed in Table I, XRD ω–2Θ characterization of EuSe films grown on GaAs(111)B substrates, wide XRD scans of EuSe/Bi_2Se_3 films, growth and properties of trilayer EuSe/Bi_2Se_3/EuSe films, details of magnetic measurements and analysis, and phase diagram for a (111) EuSe/BaF_2 film.

AUTHOR DECLARATIONS

Conflict of Interest

The authors have no conflicts to disclose.

Author Contributions

Y.W. and X.L. contributed equally to this work.

DATA AVAILABILITY

The data that support the findings of this study are available from the corresponding author upon reasonable request.

REFERENCES

[1] Y. Tokura, K. Yasuda, and A. Tsukazaki, "Magnetic topological insulators," Nat. Rev. Phys. **1**, 126–143 (2019).

[2] P. Chen et al., "Tailoring the hybrid anomalous Hall response in engineered magnetic topological insulator heterostructures," Nano Lett. **20**, 1731–1737 (2020).

[3] S.-J. Chang et al., "Heterostructured ferromagnet-topological insulator with dual-phase magnetic properties," RSC Adv. **8**, 7785–7791 (2018).

[4] R. Yu et al., "Quantized anomalous Hall effect in magnetic topological insulators," Science **329**, 61–64 (2010).

[5] M. Mogi et al., "Magnetic modulation doping in topological insulators toward higher-temperature quantum anomalous Hall effect," Appl. Phys. Lett. **107**, 182401 (2015).

[6] D. Xiao et al., "Realization of the axion insulator state in quantum anomalous Hall sandwich heterostructures," Phys. Rev. Lett. **120**, 056801 (2018).

[7] L. Fu and C. L. Kane, "Superconducting proximity effect and Majorana fermions at the surface of a topological insulator," Phys. Rev. Lett. **100**, 096407 (2008).

[8] P. Wei et al., "Exchange-coupling-induced symmetry breaking in topological insulators," Phys. Rev. Lett. **110**, 186807 (2013).

[9] F. Katmis et al., "A high-temperature ferromagnetic topological insulating phase by proximity coupling," Nature **533**, 513–516 (2016).

[10] J. Chen et al., "Evidence for magnetic skyrmions at the interface of ferromagnet/topological-insulator heterostructures," Nano Lett. **19**, 6144–6151 (2019).

[11] F. Wang et al., "Observation of interfacial antiferromagnetic coupling between magnetic topological insulator and antiferromagnetic insulator," Nano Lett. **19**, 2945–2952 (2019).

[12] Q. L. He et al., "Tailoring exchange couplings in magnetic topological-insulator/antiferromagnet heterostructures," Nat. Mater. **16**, 94–100 (2017).

[13] C. Lei, H. Chen, and A. H. MacDonald, arXiv:2107.02307 (2021).

[14] A. Mauger and C. Godart, "The magnetic, optical, and transport properties of representatives of a class of magnetic semiconductors: The europium chalcogenides," Phys. Rep. **141**, 51–176 (1986).

[15] W. L. Roth, "Neutron and optical studies of domains in NiO," J. Appl. Phys. **31**, 2000–2011 (1960).

[16] H. Kondoh and T. Takeda, "Observation of antiferromagnetic domains in nickel oxide," J. Phys. Soc. Jpn. **19**, 2041–2051 (1964).

[17] T. Yamada, "Magnetic anisotropy, magnetostriction, and magnetic domain walls in NiO. I. Theory," J. Phys. Soc. Jpn. **21**, 664–671 (1966).

[18] S. Saito, M. Miura, and K. Kurosawa, "Optical observations of antiferromagnetic S domains in NiO (111) platelets," J. Phys. C: Solid State Phys. **13**, 1513–1520 (1980).

[19] K. Nakahigashi, N. Fukuoka, and Y. Shimomura, "Crystal structure of antiferromagnetic NiO determined by x-ray topography," J. Phys. Soc. Jpn. **38**, 1634–1640 (1975).

[20] G. A. Slack, "Crystallography and domain walls in antiferromagnetic NiO crystals," J. Appl. Phys. **31**, 1571–1582 (1960).

[21] R. T. Lechner et al., "Strain induced changes in the magnetic phase diagram of metamagnetic heteroepitaxial EuSe/$PbSe_{1-x}Te_x$ multilayers," Phys. Rev. Lett. **94**, 157201 (2005).

[22] R. T. Lechner et al., "Spin configurations in strained magnetic EuSe/$PbSe_{1-x}Te_x$ superlattices grown by molecular beam epitaxy," Physica E **32**, 379–382 (2006).

[23] R. Griessen, M. Landolt, and H. R. Ott, "A new antiferromagnetic phase in EuSe below 1.8 K," Solid State Commun. **9**, 2219–2223 (1971).

[24] U. Köbler et al., "Biquadratic exchange interactions in the europium mono-chalcogenides," Z. Phys. B Condens. Matter **100**, 497–506 (1996).

[25] J. S. Moodera, R. Meservey, and X. Hao, "Variation of the electron-spin polarization in EuSe tunnel junctions from zero to near 100% in a magnetic field," Phys. Rev. Lett. **70**, 853–856 (1993).

[26]A. B. Henriques *et al.*, "Band-edge polarized optical absorption in europium chalcogenides," Phys. Rev. B **72**, 155337 (2005).

[27]K. Prokeš *et al.*, "Search for enhanced magnetism at the interface between Bi_2Se_3 and EuSe," Phys. Rev. B **103**, 115438 (2021).

[28]B. Díaz *et al.*, "Magnetic ordering and transitions of EuSe studied by x-ray diffraction," Phys. Rev. B **81**, 184428 (2010).

[29]X. Liu, J. Wang, L. Riney, S. K. Bac, D. J. Smith, M. R. McCartney, I. Khan, A. J. Hoffman, M. Dobrowolska, and J. B. A. A. Furdyna, "Unraveling the structural and electronic properties of the strained PbSe on GaAs," J. Cryst. Growth **570**, 126235 (2021).

[30]A. Richardella *et al.*, "Coherent heteroepitaxy of Bi_2Se_3 on GaAs (111)B," Appl. Phys. Lett. **97**, 262104 (2010).

[31]X. Liu *et al.*, "Structural properties of Bi_2Te_3 and Bi_2Se_3 topological insulators grown by molecular beam epitaxy on GaAs(001) substrates," Appl. Phys. Lett. **99**, 171903 (2011).

[32]S. Vishwanath *et al.*, "Controllable growth of layered selenide and telluride heterostructures and superlattices using molecular beam epitaxy," J. Mater. Res. **31**, 900–910 (2016).

[33]R. Kirchschlager, W. Heiss, R. T. Lechner, G. Bauer, and G. Springholz, "Hysteresis loops of the energy band gap and effective *g* factor up to 18 000 for metamagnetic EuSe epilayers," Appl. Phys. Lett. **85**, 67 (2004).

[34]I. Suzuki, T. Koike, M. Itoh, T. Taniyama, and T. Sato, "Stability of ferromagnetic state of epitaxially grown ordered FeRh thin films," J. Appl. Phys. **105**, 07E501 (2009).

[35]S. P. Bennett *et al.*, "Direct evidence of anomalous interfacial magnetization in metamagnetic Pd doped FeRh thin films," Sci. Rep. **5**, 9142 (2015).

[36]S. P. Bennett *et al.*, "Giant controllable magnetization changes induced by structural phase transitions in a metamagnetic artificial multiferroic," Sci. Rep. **6**, 22708 (2016).